

# Qualitative relation between reflected light intensity by Kalliroscope flakes and velocity field in the Couette–Taylor flow system

N. Abcha · N. Latrache · F. Dumouchel · I. Mutabazi

Received: 27 March 2007 / Revised: 21 December 2007 / Accepted: 8 January 2008 / Published online: 9 February 2008  
© Springer-Verlag 2008

**Abstract** We have used particle image velocimetry adapted to the Couette–Taylor system in order to measure the flow characteristics (axial and radial velocity components, vorticity fields, kinetic energy, etc.) and their spatio-temporal dependence. By looking for similarity between spatio-temporal diagrams of reflected light intensity and those of velocity fields, we have established that the intensity of light reflected by Kalliroscope flakes is related to the radial velocity component when the outer cylinder is fixed.

## Abbreviations

CCF	Circular Couette flow
TVF	Taylor vortex flow
WVF	Wavy vortex flow
MWVF	Modulated wavy vortex flow
TTVF	Turbulent Taylor vortex flow

## List of symbols

$L$	cylinder length (cm)
$a$	inner cylinder radius (cm)
$b$	outer cylinder radius (cm)
$d$	size gap (cm)
$Re$	Reynolds number
$Ta$	Taylor number
$n$	optical refraction index
$v_r$	radial velocity component (m/s)
$v_z$	axial velocity component (m/s)

$\Delta t_{\text{res}}$	residence time (s)
Abs	absolute value

## Greek symbols

$\Gamma$	aspect ratio
$\eta$	radius ratio
$\Omega$	angular velocity (rad/s)
$\xi$	dimensionless radial coordinate
$\zeta$	dimensionless axial coordinate
$\nu$	Kinematic viscosity (m <sup>2</sup> /s)
$\rho$	fluid density (g/cm <sup>3</sup> )
$\lambda$	pattern wavelength

## 1 Introduction

Experimental investigation of flow regimes makes extended use of visualization techniques by seeding the flow with fluorescent or anisotropic particles (Van Dyke 1982). Fluorescent dye, often used in visualization of open flows, appears to be not suitable for closed flows as rapidly the flow will become entirely colored and no flow structure can be caught. That is the reason why anisotropic particles such as aluminium powders or Kalliroscope flakes are of a better use in closed flows like the Couette–Taylor flow (Taylor 1923; Coles 1965; Matisse and Gorman 1984; Dominguez-Lerma 1985). They allow for direct visualization of the vortex structure in the azimuthal and axial directions or their section by a laser light. They have been used in different flow systems for investigation of vortex pattern in Rayleigh–Bénard convection (Koschmieder 1993) or in plane Couette flow (Hegseth 1996). Visualization by anisotropic particles allows for a qualitative characterization of general features of the flow. In particular, spatio-temporal evolution can be caught using appropriate signal

N. Abcha · N. Latrache · F. Dumouchel · I. Mutabazi (✉)  
Laboratoire de Mécanique, Physique et Géosciences,  
Université du Havre, 25 rue Philippe Lebon, B.P. 540,  
76058 Le Havre Cedex, France  
e-mail: mutabazi@univ-lehavre.fr

processing techniques such as space–time diagrams developed in the last decade.

The Couette–Taylor system is composed of two coaxial differentially rotating cylinders; it represents a good prototype for the investigation of centrifugal instabilities and the transition to turbulence in closed flows. This flow system has been subject of intense studies since the pioneering work of Taylor (1923). Since then, many theoretical and experimental studies have been performed (Chandrasekhar 1961; Swinney and Gollub 1981; Van Dyke 1982; Andereck et al. 1986; Chossat and Iooss 1994; Tagg 1994). In experimental studies, flow patterns have been mostly visualized by means of anisotropic aluminium powder (Koschmieder 1993) or by a suspension of Kalliroscope flakes (Coles 1965; Gorman and Swinney 1982; Matisse and Gorman 1984). It has been shown in such studies that the Couette–Taylor system exhibits a rich variety of flow patterns depending on geometrical (aspect ratio and radius ratio) and physical parameters (flow viscosity, cylinder rotation speeds). Because of the intensive use of these particles in the investigation of flows in closed systems, theoretical and experimental attempts have been made to relate the flow properties to the visualized structures by anisotropic particles (Matisse and Gorman 1984; Dominguez-Lerma 1985; Savas 1985; Gauthier et al. 1998; Thoroddsen and Bauer 1999). Since 2 decades, the visualization techniques have been complemented with laser doppler velocimetry (LDV) (Ahlers et al. 1986; Wereley and Lueptow 1994), ultrasonic doppler velocimetry (UDV) (Takeda et al. 1993; Takeda 1999) and particle image velocimetry (PIV) (Wereley and Lueptow 1998; Wereley and Lueptow 1999; Wereley et al. 2002; Hwang and Yang 2004) in order to obtain quantitative data. Each velocimetry technique has its own limitation: LDV gives a time-averaged velocity in a point, the UDV provides a velocity profile along a line and the PIV gives a velocity field in relatively limited flow cross section.

The visualization and the velocimetry represent important investigation tools in Fluid Dynamics. Unfortunately, no clear answer has been provided so far to the following question: which flow information is given by the Kalliroscope particles? To our knowledge the only studies that have tried to answer this question are the work of Savas (1985) and that of Gauthier et al. (1998). Savas assumed that thin axisymmetric particles align themselves onto the “stream surfaces” in the case of plane Couette flow. He then calculated the reflected light intensity in the flow existing far above a rotating disk, where it can be approximated locally by a unidirectional flow. Under this assumption, it was possible to follow the orientation of a particle along a streamline. This orientation gives only access to one of the three eigenvalues of the velocity gradient tensor. Gauthier et al. (1998) have computed the

motion of triaxial ellipsoids embedded in a three-dimensional (3D) flow. They used these results to simulate the cross-section visualizations of 3D flows (Taylor–Couette flow and flow between rotating disks). The simulated visualizations for the Taylor vortex flow (TVF) regime were compared with experimental ones, and the corresponding light reflected intensity profile was found to be in rather good agreement with the numerically computed radial velocity.

The aim of the present work is to confirm this result using more precise comparison between space–time diagrams obtained using visualisation by Kalliroscope flakes and PIV. We have chosen the Kalliroscope flakes because of their optical properties; in particular they provide a better contrast of the vortex pattern structure than other tested particles.

A PIV technique, adapted in the Couette–Taylor system, was developed and used to measure the axial and radial velocity components. This allowed a quantitative characterization of each instability mode, from TVF, to TTVF. We have developed a new technique of construction of spatio-temporal diagrams from the PIV measurement of velocity fields [radial and axial velocity in the  $(r,z)$  plane]. These quantitative results were compared with those obtained from the space–time diagrams acquired by direct visualization of flow with Kalliroscope flakes.

The paper is organized as follows: after the description of experimental setup and procedure (visualization, PIV), we present the main results and then discussions before concluding remarks.

## 2 Experimental apparatus

The experimental system consists of two vertical coaxial cylinders, immersed in a large square Plexiglas box filled with water in order to maintain a controlled temperature (Fig. 1). This square box also allows for minimization of distortion effects of refraction due to curvature of the outer cylinder during optical measurements. The inner cylinder made of aluminum has a radius  $a = 4$  cm, the outer cylinder made of glass has a radius  $b = 5$  cm, the gap between the cylinders is  $d = b - a = 1$  cm and the working height is  $L = 45.9$  cm. Therefore the radius ratio  $\eta = a/b = 0.8$  and the aspect ratio is  $\Gamma = L/d = 45.9$ . The inner cylinder is rotated by a servomotor at controlled angular rotation frequency  $\Omega$  while the outer cylinder is fixed. The control parameter is the Taylor number

$$Ta = Re\sqrt{\frac{d}{a}}$$

where  $Re = \Omega ad/\nu$  is the Reynolds number and  $\nu$  is the kinematic viscosity of the working fluid. In our

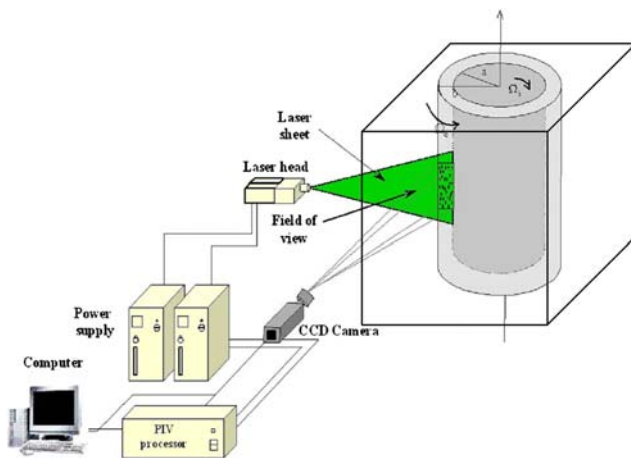


**Fig. 1** Experimental apparatus: scheme of visualization and data acquisition system

experiments, we have used deionized water for which  $\nu = 0.98 \times 10^{-2} \text{ cm}^2/\text{s}$  at the temperature  $T = 21.2^\circ\text{C}$ .

## 2.1 Visualization by Kalliroscope platelets and space–time diagrams

For the visualization of flow structures, we have added 2% volume of Kalliroscope AQ1000, which is a suspension of 1–2% of reflective flakes of a typical size of  $30 \mu\text{m} \times 6 \mu\text{m} \times 0.07 \mu\text{m}$  (Matisse and Gorman 1984; Dominguez-Lerma 1985) with a relatively large reflective optical index  $n = 1.85$  and a density of  $\rho = 1.62 \text{ g/cm}^3$ . The sedimentation of these particles remains negligible in horizontal or vertical configurations if the experiment lasts less than 10 h (Matisse and Gorman 1984) because their sedimentation velocity is  $v_s = 2.8 \times 10^{-5} \text{ cm/s}$ . These particles do not modify significantly the flow viscosity and no non-Newtonian effect was detected as far as small concentrations ( $c < 5\%$ ) are used (Dominguez-Lerma 1985; Noir 2000). The choice of the concentration of 2% was done to ensure the best contrast in the flow. The values of the control parameter ( $Ta$ ) are determined within a precision of 2%.

Using a He–Ne Laser sheet ( $\lambda = 632 \text{ nm}$ , 1-mm wide beam, spread by a cylindrical lens), it was possible to visualize the cross section of the flow in the  $r$ – $z$  plane. Figure 2 gives the cross section of regimes observed in the Couette–Taylor system for different values of the control parameter ( $Ta$ ). We have recorded with the linear CCD camera of 1,024 pixels, at regular time intervals, a reflected light intensity  $I(z)$  from a line in the center of the flow cross-section ( $r = a + d/2$ ), parallel to the cylindrical axis. The recorded length varies from 25 to 29 cm in the central part of the system, corresponding to a spatial resolution from 40 to 30 pixels/cm. The intensity was sampled over a 256 values range, displayed in gray levels at regular time

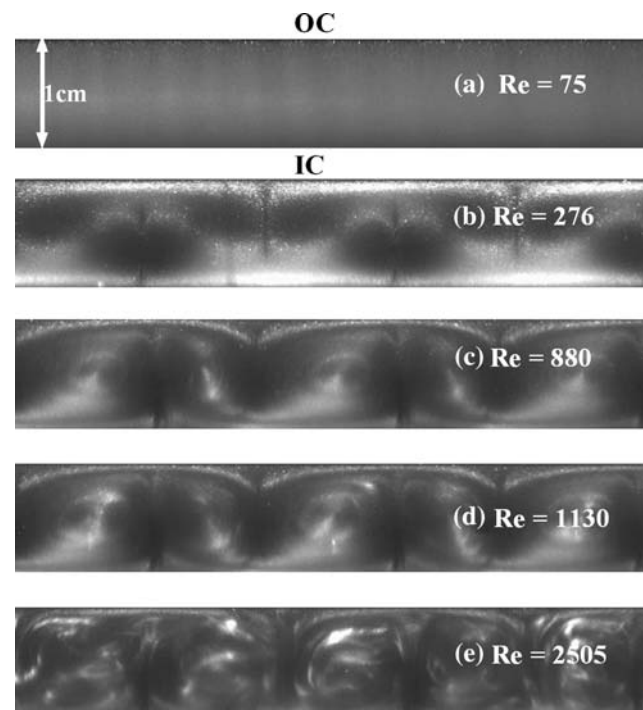


**Fig. 2** Cross-section of the flow regimes visualized using Kalliroscope flakes: CF, TVF, WVF, MWVF and TTVF

intervals in order to produce space–time diagrams  $I(z,t)$  of the pattern which shows the temporal and spatial evolution of vortices (Fig. 3). This procedure allows for a good resolution in vortex oscillation frequencies since the time can be chosen as long as the storage capacity allows (Fig. 4).

To record the motion in the radial direction, we have used a 2-D IEEE1394 camera (A641f, Basler) and have recorded the cross-sections in the  $(r,z)$  plane. We extracted the radial distribution of the light intensity at regular time interval and then plotted the space–time diagram  $I(r,t)$  (Fig. 5).

The technique of space–time diagrams does not provide quantitative data on the velocity or vorticity fields that are important for the estimate of energy or momentum transfer in the different regimes.

## 2.2 PIV measurements

For PIV measurements, the flow was seeded with spherical glass particles of diameter 8–11  $\mu\text{m}$  and density  $\rho = 1.6 \text{ g/cm}^3$ , in concentration of about  $10^{-4}\%$  (1 ppm) per mass. The PIV system consists of two Nd:YAG Laser sources, a MasterPiv processor (from Tecflow) and a CCD camera (Kodak) with  $1,034 \times 779$  pixels. In the PIV technique, the flow in the test area of the plane  $(r,z)$  is visualized with a thin light sheet which illuminates the glass particles, the positions of which can be recorded at short time intervals.

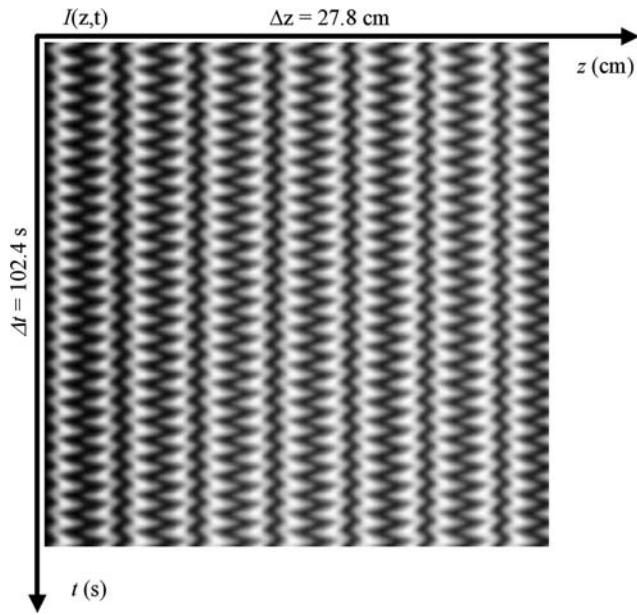


**Fig. 3** Space–time diagrams for wavy vortex flow (WVF) ( $Ta = 440$ ): axial distribution  $I(z,t)$

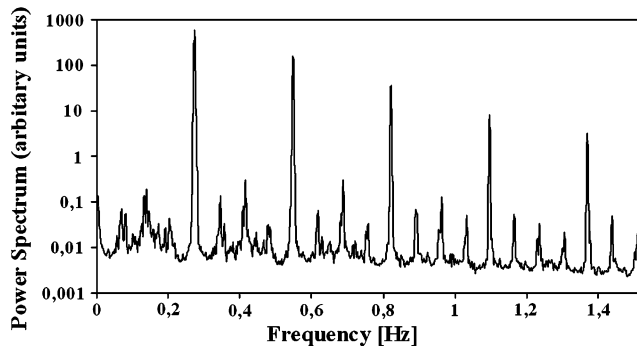


**Fig. 4** Power spectrum frequency for a WVF observed at  $Ta = 440$

The thickness of the laser sheet is  $e = 1$  mm and the residence time of the particles can be estimated as  $\Delta t_{res} \sim 10/Re$ . The interframe delay (time delay between two Laser pulses) must be chosen much smaller than  $\Delta t_{res}$  depending on the values of the Reynolds number, it varies from 0.5 to 25 ms for the investigated flow regimes. The temporal duration of each of the two laser pulses is of 7 ns over the interframe delay leading to a negligible error on the velocity measurements. We have recorded 195 pairs of images of size  $1,034 \times 779$  pixels. Each image of a pair was sampled into windows of  $32 \times 32$  pixels with a recovering of 50%. The velocity fields were computed using the intercorrelation method, which is implemented in the software “Corelia-V2IP” (Tecflow). The spatial intercorrelation of images is represented by a “likelihood function” of a chosen window with respect to another; and is calculated as follows (Lecerf 2000):

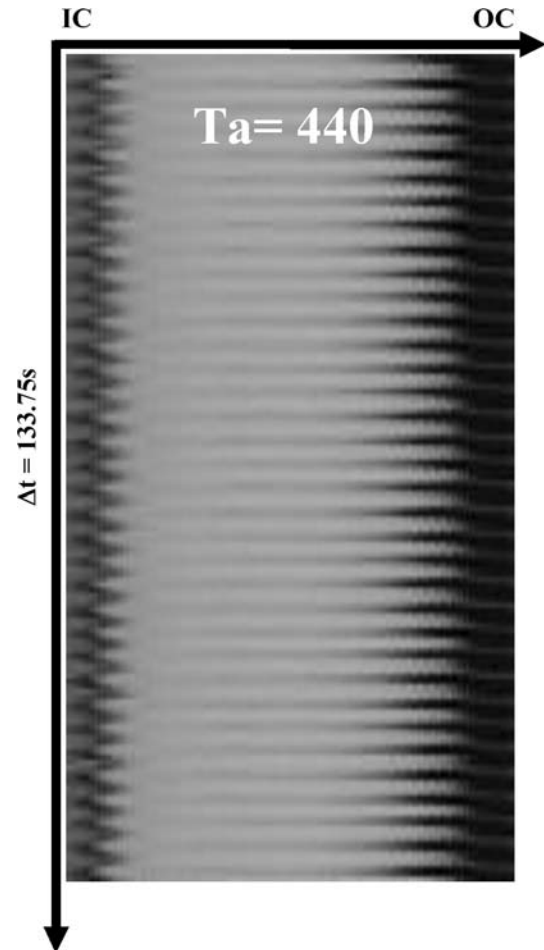


**Fig. 5** Space–time diagram for a WVF ( $Ta = 440$ ): radial distribution  $I(r,t)$

$$CC_{I_1 I_2}(\vec{s}) = \frac{\sum_{\vec{x}} (I_1(\vec{x}) - \mu_1) \cdot I_2(\vec{x} + \vec{s}) - \mu_2}{\sqrt{\sigma_1 \sigma_2}}$$

where  $\mu_1, \mu_2$  are the averages and  $\sigma_1, \sigma_2$  represent the standard deviations of the functions  $I_1, I_2$  which represent the interrogation windows of the first and second images, respectively;  $\vec{x}$  and  $\vec{x} + \vec{s}$  represent two distinct positions in

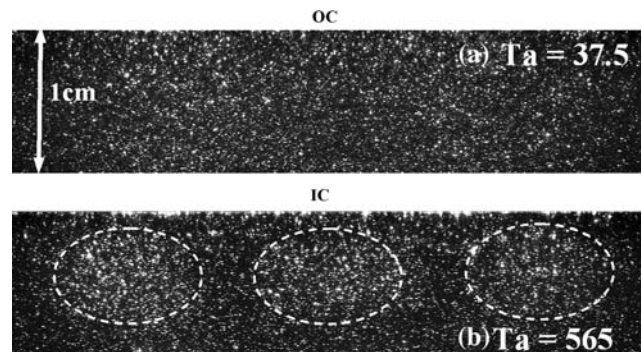


**Fig. 6** Cross section of flow visualized with glass particles for: **a** the CCF ( $Ta = 37.5$ ), **b** the MWVF ( $Ta = 565$ )

space. The worst estimate of the error on the particle displacement measurement is about  $\pm 0.1\%$ . The delay between the two consecutive images in a pair allows for determination of the flow local velocity (with an error of  $\pm 0.1\%$ ).

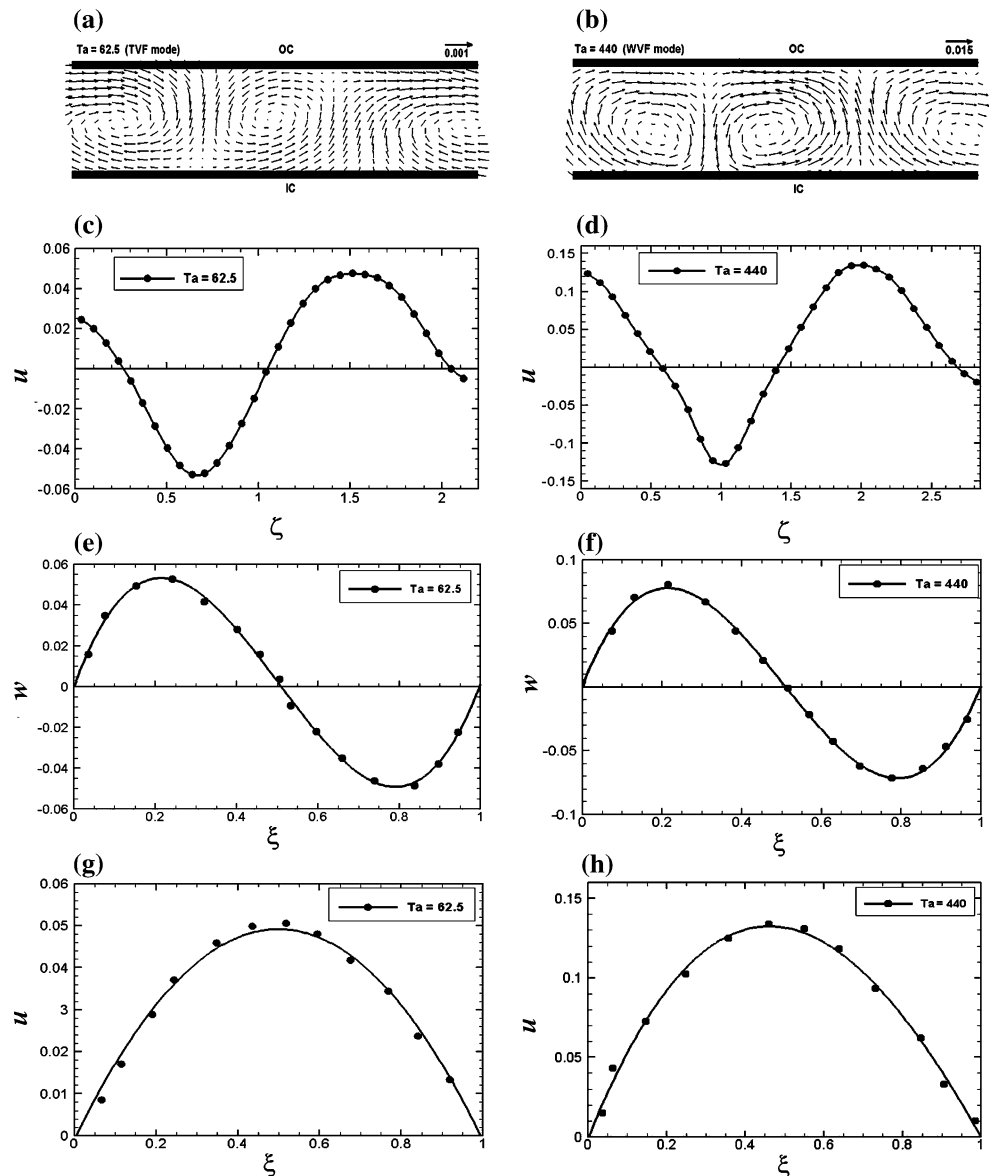
We have performed PIV measurements in the circular Couette flow (CCF), in the TVF and wavy vortex flow (WVF) regimes in order to check our data acquisition system and to compare with the data available in the literature for the three regimes (Wereley and Lueptow 1998; Hwang and Yang 2004). In the circular Couette flow, the spherical glass particles are uniformly distributed (Fig. 6a) while in the TVF and WVF, after 10 h, the particles have migrated towards the vortex cores where the radial velocity vanishes (Fig. 6b).

The result of the complete process is illustrated by 2D velocity fields of Fig. 7. The inflow and outflow are clearly evidenced in the case of the TVF and WVF.

### 3 Results and discussion

The PIV allows for the visualization of flow streamlines in the cross section  $(r,z)$ . The measured radial and axial velocity components  $v_r(r)$ ,  $v_z(r)$  at a given axial position ( $\zeta = z/d$ ) or  $v_r(z)$  and  $v_z(z)$  at a given radial position ( $\xi = (r - a)/d$ ) are plotted in Fig. 7 for the TVF and WVF. The radial and axial velocity components have been fitted by a polynomial function satisfying the non-slip condition at the cylindrical wall ( $\xi = 0$ ,  $\xi = 1$ ). We have

**Fig. 7** a, b Velocity field from PIV measurement. c–h Dimensionless radial and axial velocity profiles for TVF ( $Ta = 62.5$ ), WVF ( $Ta = 440$ ) where  $u = v_r/\Omega a$ ,  $w = v_z/\Omega a$



calculated the time-averaged velocity components in the axial and radial directions (Fig. 7c–h). From these velocity profiles, we have deduced different quantities characterizing the flow perturbations in the cross section ( $r, z$ ) for each regime (Fig. 8):

- the vorticity  $\omega = (\partial v_r / \partial z - \partial v_z / \partial r) / 2$
- the kinetic energy  $E = (v_r^2 + v_z^2) / 2$

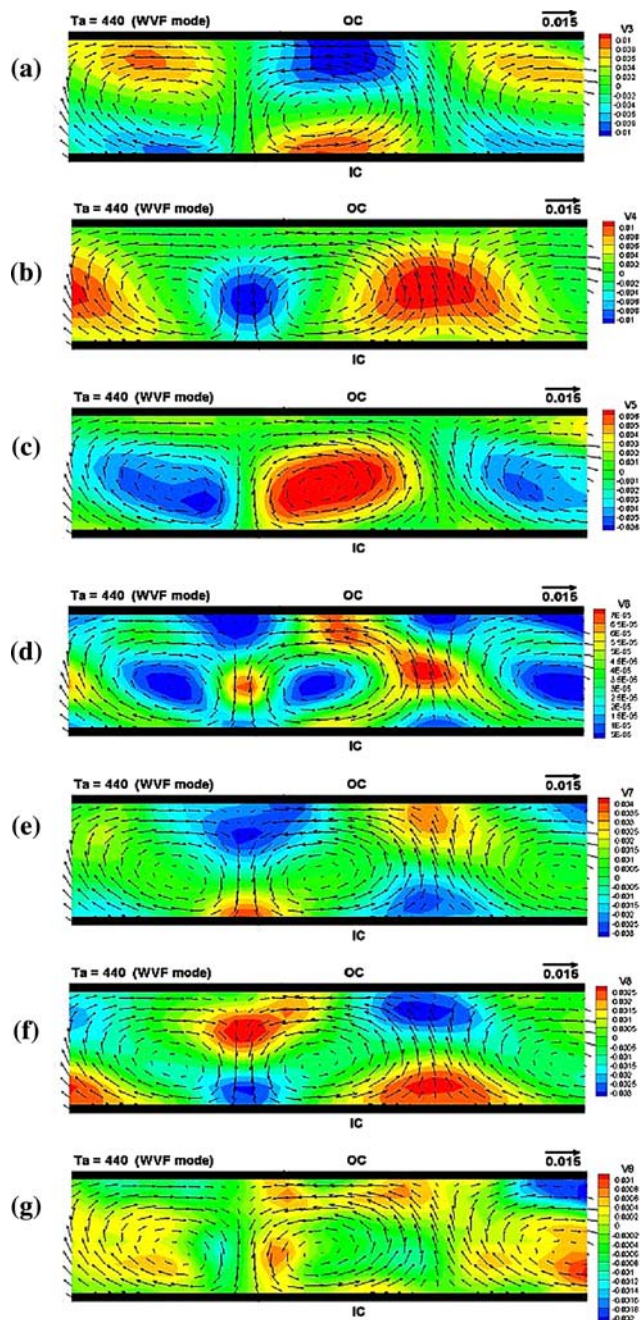


**Fig. 8** Field of flow quantities in the cross section ( $r, z$ ) for WVF: **a** axial velocity; **b** radial velocity; **c** vorticity; **d** kinetic energy; **e** axial elongation; **f** radial elongation; **g** shear rate

- three components of the shear rate tensor:

$$\dot{\epsilon}_{rr} = \partial v_r / \partial r, \quad \dot{\epsilon}_{zz} = \partial v_z / \partial z, \quad \dot{\epsilon}_{rz} = (\partial v_r / \partial z + \partial v_z / \partial r) / 2$$

The vorticity fields and velocity components show that inflow and outflow are almost symmetric in the TVF while they are dissymmetric in the WVF because of the oscillations of the separatrices. The radial velocity reaches the maximal value in the middle of the gap and vanishes at the cylinder walls.

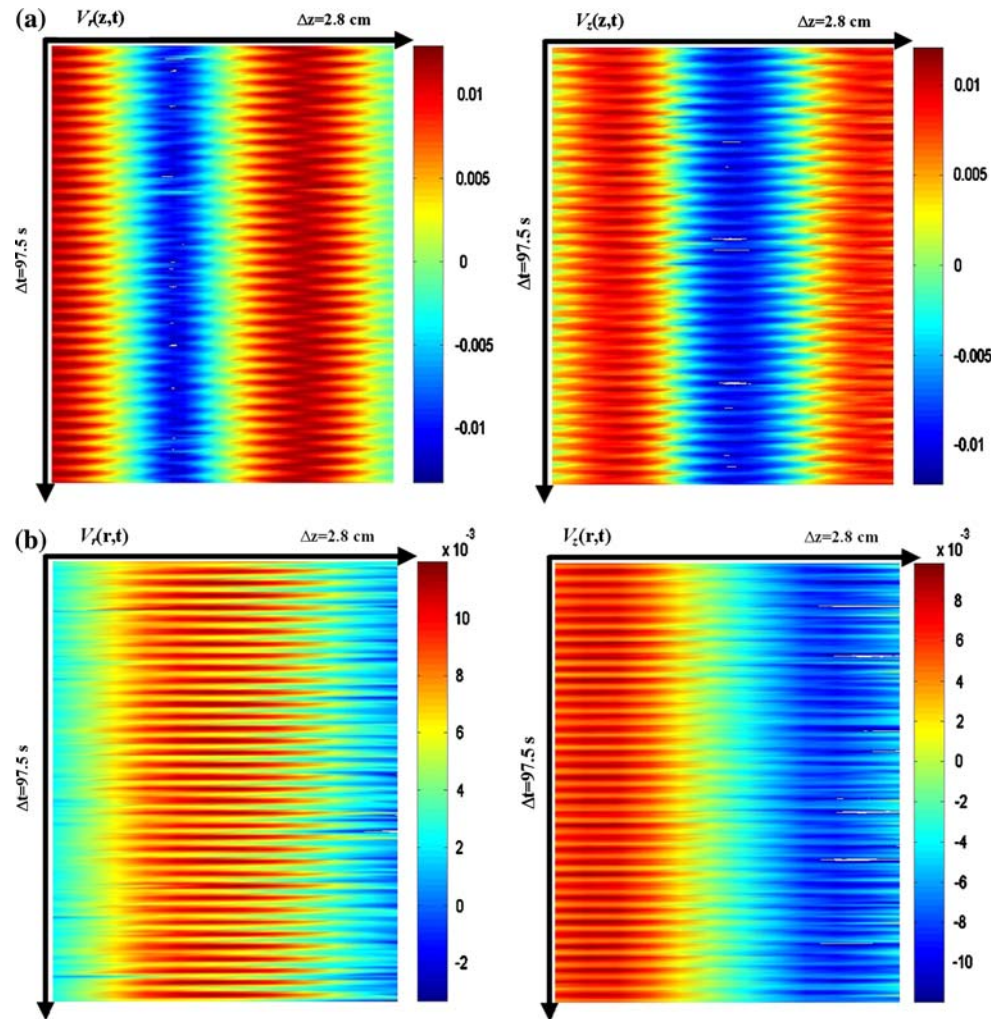
The instantaneous velocity components can be superposed chronologically at regular time intervals in order to obtain space–time diagrams (Fig. 9). The resulting diagrams are color coded as follows: the red color corresponds to positive values and blue to the negative values of the velocity. For example in Fig. 9a, the red color corresponds to the outflow and the blue color to the inflow. In Fig. 9b, the red color corresponds to the anti-clockwise vortex core and the blue color to the clockwise vortex core.

In Figs. 10a and 11a, we have compared the space–time diagrams obtained from PIV measurements (Fig. 9a) with those obtained from flow visualization by Kalliroscope flakes in both directions for a wavy vortex regime at  $Ta = 440$ . One must keep in mind that, unlike space–time diagrams of velocities components, space–time diagrams obtained from the reflected light intensity do not give any information about the flow direction [upward or downward for  $I(z, t)$ , inward vs. outward for  $I(r, t)$ ]. Hence, for comparison, we have used the absolute values of the velocity components obtained by PIV.

At first glance, we have realized that the space–time diagrams obtained by Kalliroscope flakes are very similar with those of the radial velocity component  $v_r(z, t)$  and  $v_r(r, t)$ . Figures 10b and 11b illustrate the time-average profiles in the axial and radial directions. These plots highlight the fact that Kalliroscope particles give a signature of the radial velocity component measured in the centre of the gap ( $\xi = 0.5$ ). The minima and maxima are reached for identical axial positions. A similar correspondence is obtained with the envelopes of the space–time diagrams in the axial and radial directions and leads to the same conclusion (Figs. 10b, 11b): a perfectly identical evolution in the annular space, a maximum reached in the middle of the gap and minima at the walls of two cylinders. Moreover, the absolute value of the radial velocity vanishes in the vortex core while it reaches the maximum in the outflow and in the inflow. The reflected light intensity vanishes in the vortex core because the weak motion of Kalliroscope flakes. In the inflow and outflow where the Kalliroscope flakes are faster in the radial direction, the intensity is much larger than in the other parts of the flow.

Recent numerical simulations (Gauthier et al. 1998) have shown that the Kalliroscope or iriodin particles may

**Fig. 9** **a** Space–time diagrams for  $Ta = 440$ :  $v_r(z,t)$  taken at  $\xi = 0.5$ ,  $v_z(z,t)$  at  $\xi = 0.25$  or  $\xi = 0.75$ . **b** Space–time diagrams for  $Ta = 440$ :  $v_r(r,t)$  at outflow position,  $v_z(r,t)$  in the core of anticlockwise vortex (positive vorticity)



be related to the radial velocity component but no measurements were provided to sustain these arguments. Using their estimates of characteristic times of the anisotropic particles in flow, we have found that the relaxation time  $\tau$  of the Kalliroscope flakes is about  $0.01T_p$ , where the precession time  $T_p \sim d/v_r \sim d/v_z \approx 2$  s for the TVF and  $T_p \approx 1$  s for WVF. The time scale of the Brownian orientation in a water flow is about 100 s at room temperature (Savas 1985), it is large enough compared to other time scales of our experiment so that the Brownian motion can be neglected. The comparison of the space–time diagrams obtained from flow visualization and PIV measurements performed for different flow regimes has allowed us to confirm that in the case of the fixed outer cylinder the reflective particles in the flow give information on the radial velocity component. Therefore, the commonly admitted conjecture that the reflective particles give information on the shear rate (Savas 1985) is in contradiction with the quantitative results. In fact, we have plotted in Fig. 12 profiles of different flow properties in the axial and radial direction. None of them has a similar

behaviour as the reflected light intensity profile (Figs. 10b, 11b). Our results give a more precise content on the fact the small anisotropic particles align with the flow streamlines (Savas 1985; Gauthier et al. 1998; Matisse and Gorman 1984) by giving the precision on the velocity component which bears these alignment.

One should mention that our results were verified for TVF, WVF and MWVF in which the radial velocity component has a magnitude a little larger than that of the axial component. For turbulent Taylor vortex flow (TTVF), no conclusive observation has been made. Following the results from Gauthier et al. (1998) one would expect the applicability of the present results to pre-turbulent patterns observed in flow between differentially rotating discs (Cros and Le Gal 2002).

#### 4 Conclusion

We have performed experiment to determine the quantitative information provided by Kalliroscope flakes used

**Fig. 10** **a** Space–time diagrams of the intensity distribution in the axial  $I(z,t)$  and radial  $I(r,t)$  direction for  $Ta = 440$ . **b** Radial profile and axial profile of light reflected intensity  $I/I_{\max}$  taken at  $\xi = 0.5$

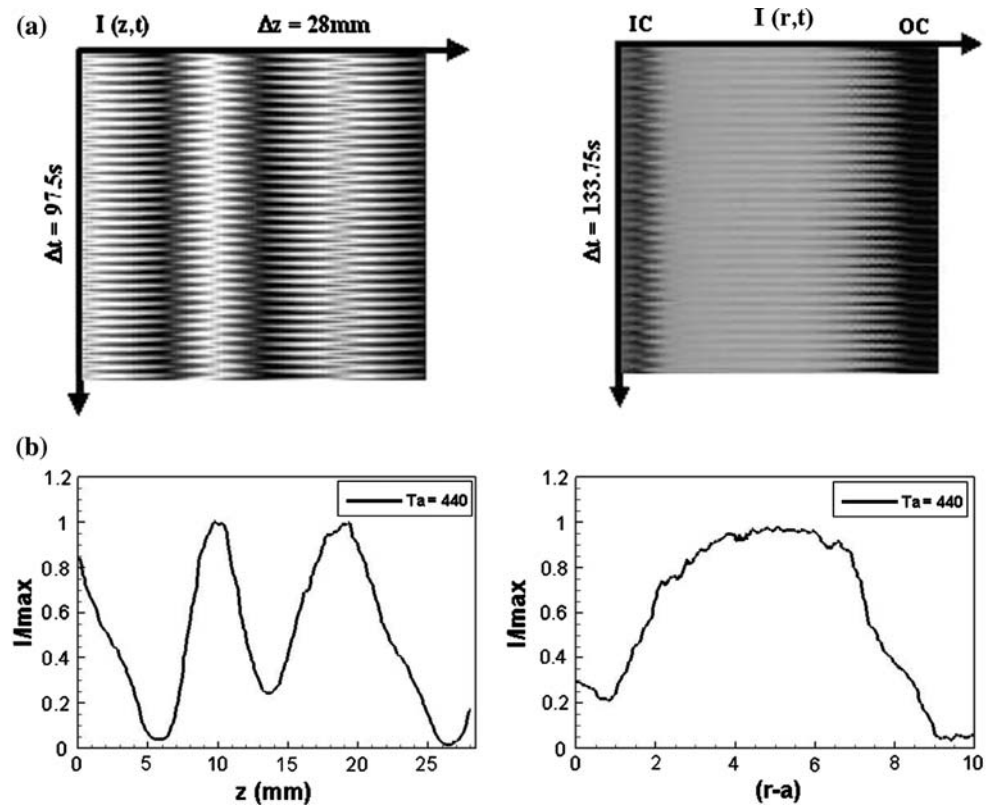


**Fig. 11** **a** Space–time diagrams of the absolute value of radial velocity component for  $Ta = 440$ . **b** Radial and axial profiles of the absolute value of the radial velocity component measured at  $\xi = 0.5$

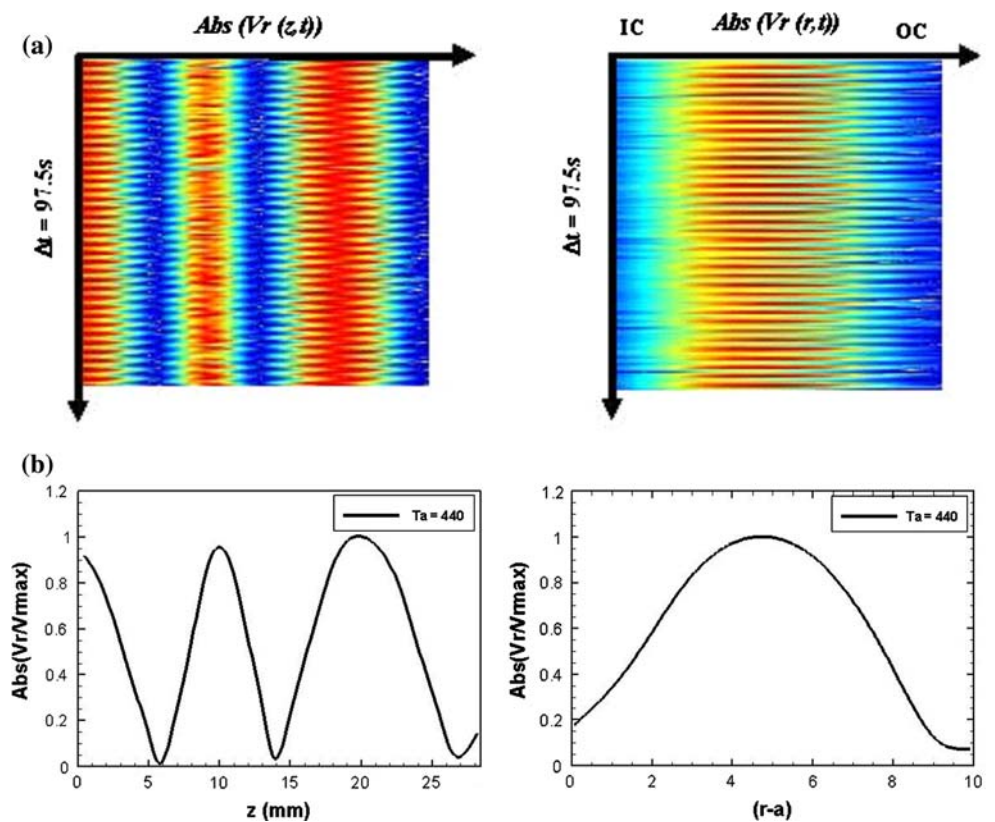
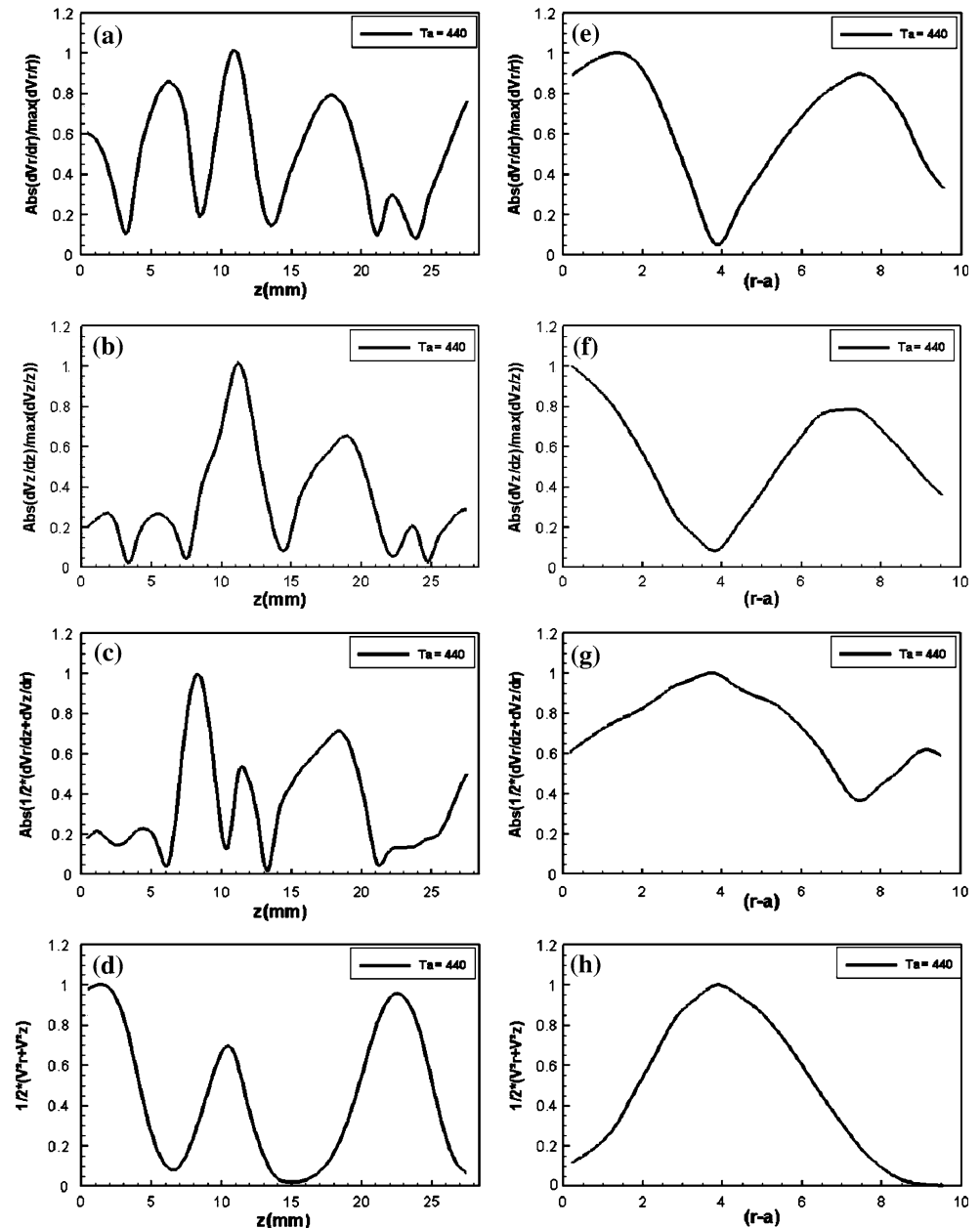




**Fig. 12** Axial profiles of the absolute values of flow characteristics measured at  $\zeta = 0.5$ : **a**  $\hat{e}_{rr}$ , **b**  $\hat{e}_{zz}$ , **c**  $\hat{e}_{rz}$  and **d** kinetic energy  $E$ . Radial profiles of the absolute values of flow characteristics measured in the outflow: **e**  $\hat{e}_{rr}$ , **f**  $\hat{e}_{zz}$ , **g**  $\hat{e}_{rz}$  and **h** kinetic energy  $E$



for visualization of vortex structure in the Couette–Taylor system with a fixed outer cylinder. Using PIV technique, we have determined different flow characteristics (velocity, vorticity, shear strain and kinetic energy) in the cross-section for different regimes (TVF, WVF, MWVF and TTVF). A simultaneous comparison of space–time diagrams obtained from both Kalliroscope visualization technique and PIV measurements has allowed us to compare the reflected light intensity and flow properties in the Couette–Taylor flow. We have found that this intensity is related to the radial velocity component in agreement with conclusion from numerical simulations by Gauthier et al.

**Acknowledgments** We thank B. Lecordier and D. Allano for interesting discussions on the PIV technique. This work has benefited from a financial support of the CPER-Haute Normandie under the project “CNRT-Maîtrise de la Combustion dans les Moteurs”.

## References

- Ahlers GD, Cannell DS, Dominguez-Lerma MA, Heinrichs R (1986) Wavenumber selection and Eckhaus instability in Couette–Taylor flow. *Physica D* 23:202–219
- Andereck CD, Liu SS, Swinney HL (1986) Flow regimes in a circular Couette system with independently rotating cylinders. *J Fluid Mech* 164:155–183
- Chandrasekhar S (1961) *Hydrodynamic and hydromagnetic stability*, Oxford University Press, Oxford

- Chossat P, Iooss G (1994) The Couette–Taylor problem. Applied Mathematical Science, vol 102. Springer, New-York
- Coles D (1965) Transition in circular Couette flow. *J Fluid Mech* 21:385–425
- Cros A, Le Gal P (2002), Spatiotemporal intermittency in the torsional Couette flow between rotating and stationary disk. *Phys Fluids* 14:3755–3765
- Dominguez-Lerma MA, Ahlers G, Cannell DS (1985) Effects of Kalliroscope flow visualization particles on rotating Couette–Taylor flow. *Phys Fluids* 28:1204–1206
- Gauthier G, Gondret P, Rabaud M (1998) Motions of anisotropic particles: application to visualization of three-dimensional flows. *Phys Fluids* 10:2147–2154
- Gorman M, Swinney HL (1982) Spatial and temporal characteristics of modulated waves in the circular Couette system. *J Fluid Mech* 117:123–142
- Hegseth JJ (1996) Turbulent spots in plane Couette flow. *Phys Rev E* 55:4915–4923
- Hwang JY, Yang KS (2004) Numerical study of Taylor–Couette flow with an axial flow. *Comput Fluids* 33:97–118
- Koschmieder EL (1993) Bénard cells and Taylor vortices, Cambridge University Press, Cambridge
- Lecerf A (2000) Développement de la PIV stéréoscopique. Application à l'étude de la propagation de flamme en milieu confiné. Thèse de doctorat, Université de Rouen
- Matisse P, Gorman M (1984) Neutrally buoyant anisotropic particles for flow visualization. *Phys Fluids* 27:759–760
- Noir J (2000) Ecoulement d'un fluide dans une cavité en précession: approches numérique et expérimentale. Thèse de doctorat, Université de Grenoble 1
- Savas Ö (1985) On flow visualization using reflective flakes. *J Fluid Mech* 152:235–247
- Swinney HL, Gollub JP (eds) (1981) Hydrodynamic instabilities and the transition to turbulence. In: Topics in applied physics, vol 45. Springer, Berlin
- Tagg R (1994) The Couette–Taylor problem. *Nonlinear Sci Today* 4(3):1–25
- Takeda Y (1999) Quasi-periodic state and transition to turbulence in a rotating Couette system. *J Fluid Mech* 389:81–99
- Takeda Y, Fischer WE, Sakakibara J, Ohmura K (1993) Experimental observation of the quasiperiodic modes in a rotating Couette system. *Phys Rev E* 47:4130–4134
- Taylor GI (1923) Stability of a viscous liquid contained between two rotating cylinders. *Phil Trans R Soc A* 223:289–343
- Thoroddsen ST, Bauer JM (1999) Qualitative flow visualization using colored lights and reflective flakes. *Phys Fluids* 11:1702–1704
- Van Dyke M (1982) An album of fluid motion. Parabolic, Stanford
- Wereley ST, Lueptow RM (1994) Azimuthal velocity in supercritical circular Couette flow. *Exp Fluids* 18:1–9
- Wereley ST, Lueptow RM (1998) Spatio-temporal character of nonwavy and wavy Taylor–Couette flow. *J Fluid Mech* 364:59–80
- Wereley ST, Lueptow RM (1999) Inertial particle motion in a Taylor–Couette rotating filter. *Phys Fluids* 11:325–333
- Wereley ST, Akonur A, Lueptow RM (2002) Particle-fluid velocities and fouling in rotating filtration of a suspension. *J Memb Sci* 209:469–484